Cooperative Grasping and Transport using Multiple Quadrotors

Daniel Mellinger, Michael Shomin, Nathan Michael, Vijay Kumar

GRASP Laboratory,
University of Pennsylvania,
Philadelphia, PA 19104, USA
{dmel, shomin, nmichael, kumar}@seas.upenn.edu

Summary. In this paper, we consider the problem of controlling multiple quadrotor robots that cooperatively grasp and transport a payload in three dimensions. We model the quadrotors both individually and as a group rigidly attached to a payload. We propose individual robot control laws defined with respect to the payload that stabilize the payload along three-dimensional trajectories. We detail the design of a gripping mechanism attached to each quadrotor that permits autonomous grasping of the payload. An experimental study with teams of quadrotors cooperatively grasping, stabilizing, and transporting payloads along desired three-dimensional trajectories is presented with performance analysis over many trials for different payload configurations.

1 Introduction

Autonomous grasping, manipulation, and transportation of objects is a fundamental area of robotics research important to applications which require robots to interact and effect change in their environment. With recent advancements in relevant technologies and commercially available micro aerial vehicles (MAVs), the problem of autonomous grasping, manipulation, and transportation is advancing to the aerial domain in both theory and experiments. However, individual MAVs are fundamentally limited in their ability to manipulate and transport objects of any significant size. We address this limitation in this paper and consider the problem of controlling multiple quadrotor robots that cooperatively grasp and transport a payload in three dimensions.

We approach the problem by first developing a model for a single quadrotor and a team of quadrotors rigidly attached to a payload (Sect. 3). In Sect. 4, we propose individual robot control laws defined with respect to the payload that stabilize the payload along three-dimensional trajectories. We detail the design of a gripping mechanism attached to each quadrotor that permits autonomous grasping of the payload (Sect. 5). An experimental study with teams of quadrotors cooperatively grasping, stabilizing, and transporting payloads of different configurations to desired positions and along three-dimensional trajectories is presented in Sect. 6.

2 Related Literature

The problem of aerial manipulation using cables is analyzed in [1, 2] with the focus on finding robot configurations that ensure static equilibrium of the payload at a desired pose while respecting constraints on the tension. We address a different problem as the robots use "grippers" that grasp the payload via rigid connections at multiple locations. The modeling of contact constraints is considerably simpler as issues of form or force closure are not relevant. Additionally, contact conditions do not change in our case (e.g., rolling to sliding, or contact to no contact). However, the system is statically indeterminate and the coordination of multiple robots is significantly more complex than in the case when the payload is suspended from aerial robots. In particular, as the problem is over-constrained the robots must control to move in directions that are consistent with kinematic constraints.

There is extensive literature on multi-fingered grasping and legged locomotion that discusses the problem of coordinating robot actuators with kinematic constraints [3–5]. However, our work is different in many ways. First, unlike legs or fingers, we have less control over the wrenches that can be exerted at each contact. Each robot is capable of controlling propellers to exert wrenches of a fixed pitch, (i.e., a thrust and a moment proportional to the thrust, both perpendicular to the plane of the rotor). Second, the robot system can be underactuated if the planes associated with each rotor are all parallel. In fact, this is generally the case in formation flight and it may be desirable to grasp the payload at multiple points, allowing the quadrotors to be in parallel horizontal planes. Third, the control of quadrotors necessitate dynamic models that reconcile the aerodynamics of flight with the mechanics of cooperative manipulation.

In this work we take advantage of the fact that we have access to many rotors to generate the thrust necessary to manipulate payloads. A similar concept is presented in [6], where the authors propose control laws that drive a distributed flight array consisting of many rotors along a desired trajectory. However, our control methods differ considerably as we are working with quadrotor robots and must derive feedback control laws based on the control inputs required by these robots. Similar to the concept of using multiple rotors in a flight array is the development of an aerial robot with more than four rotors (as in quadrotors), such as the commercially available *Falcon* with eight rotors from Ascending Technologies, GmBH [7].

A gripping mechanism is presented in this work that enables autonomous grasping of the payload by the quadrotors. Toward this design, we build upon considerable research in the area of climbing robots which generally rely on clinging to surface asperities via microspine arrays [8]. Similar designs with microspine arrays enable aerial vehicles to perch on vertical walls [9]. These robots do not require penetration to cling to the wall. However, in our work, the normal forces required to grasp objects are much higher compared to the shear forces that are exerted on the surfaces interfacing with the spines. Using similar microspine technology, we utilize the advantages of penetration in softer material such as wood and cardboard to attach to horizontal planar surfaces.

3 Dynamic Model

3.1 Coordinate Systems

The coordinate systems are shown in Fig. 1. The world frame, $\mathbf{W}$, is defined by axes x_W, y_W, and z_W with z_W pointing upward. We consider n quadrotors rigidly attached to a body frame, $\mathbf{B}$. It is assumed that the body frame axes are chosen as the principal axes of the entire

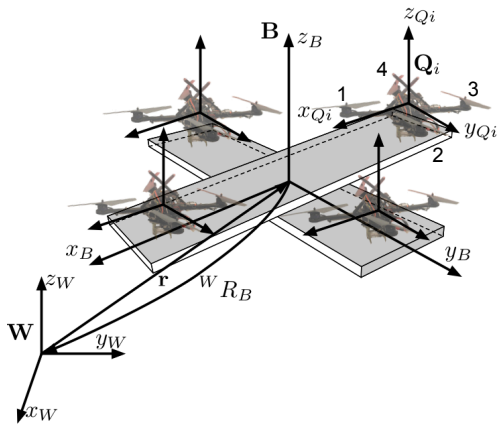

Fig. 1. The coordinate systems.

system. Each quadrotor has an individual body frame, $\mathbf{Q}_i$, attached to its center of mass with z_{Qi} perpendicular to the plane of the rotors and pointing vertically up. Let (x_i, y_i, z_i) be the coordinates of the center of mass of the i^{th} quadrotor in $\mathbf{B}$ coordinates and ψ_i be the relative yaw angle. For this quadrotor, rotor 1 is on the positive x_{Qi}-axis, 2 on the positive y_{Qi}-axis, 3 on the negative x_{Qi}-axis, 4 on the negative y_{Qi}-axis. We require the z_{Qi} axes and z_B to be parallel. We use ZXY Euler angles to model the rotation of the body (and the quadrotors) in the world frame. To get from $\mathbf{W}$ to $\mathbf{B}$, we first rotate about z_W by the yaw angle, ψ, then rotate about the intermediate x-axis by the roll angle, ϕ, and finally rotate about the y_B axis by the pitch angle, θ. The rotation matrix for transforming coordinates from $\mathbf{B}$ to $\mathbf{W}$ is given by

$$ {}^W R_B = \begin{bmatrix} c\psi c\theta - s\phi s\psi s\theta & -c\phi s\psi & c\psi s\theta + c\theta s\phi s\psi \\ c\theta s\psi + c\psi s\phi s\theta & c\phi c\psi & s\psi s\theta - c\psi c\theta s\phi \\ -c\phi s\theta & s\phi & c\phi c\theta \end{bmatrix}, $$

where $c\theta$ and $s\theta$ denote $\cos\theta$ and $\sin\theta$, respectively, and similarly for ϕ and ψ. The components of angular velocity of the body in the body frame are p, q, and r. These values are related to the derivatives of the roll, pitch, and yaw angles according to:

$$ \begin{bmatrix} p \\ q \\ r \end{bmatrix} = \begin{bmatrix} c\theta & 0 & -c\phi s\theta \\ 0 & 1 & s\phi \\ s\theta & 0 & c\phi c\theta \end{bmatrix} \begin{bmatrix} \dot{\phi} \\ \dot{\theta} \\ \dot{\psi} \end{bmatrix}. $$

The position vector of the center of mass of the body in the world frame is denoted by $\mathbf{r}$. The rotation matrix, Euler angles, angular velocities, and position vector to the center of mass of the i^{th} quadrotor are denoted as ${}^W R_{Qi}$, $(\phi_i,\, \theta_i,\, \psi_i)$, $(p_i,\, q_i,\, r_i)$, and $\mathbf{r}_i$, respectively.

3.2 Motor Model

Each rotor has an angular speed ω and produces a vertical force F according to

$$ F = k_F \omega^2. \tag{1} $$

Experimentation with a fixed rotor at steady-state shows that $k_F \approx 6.11 \times 10^{-8} N/rpm^2$. The rotors also produce a moment according to

$$M = k_M \omega^2.$$

The constant, k_M, is determined to be about $1.5 \times 10^{-9} Nm/rpm^2$ by matching the performance of the simulation to the real system.

The results of a system identification exercise suggest that the rotor speed is related to the commanded speed by a first-order differential equation:

$$\dot{\omega} = k_m(\omega^{des} - \omega).$$

This motor gain, k_m, is found to be about $20\,\mathrm{s}^{-1}$ by matching the performance of the simulation to the real system. The desired angular velocities, ω^{des}, are limited to a minimum and maximum value determined through experimentation to be approximately $1200\,\mathrm{rpm}$ and $7800\,\mathrm{rpm}$.

3.3 Equations of Motion

Each of the j rotors on each of the the i quadrotors produces a force, $F_{i,j}$, and moment, $M_{i,j}$, in the z_{Qi} direction. These rotor forces can be rewritten as a total force from each quadrotor $F_{q,i}$ as well as moments about each of the quadrotor's body frame axes:

$$\begin{bmatrix} F_{q,i} \\ M_{xq,i} \\ M_{yq,i} \\ M_{zq,i} \end{bmatrix} = \begin{bmatrix} 1 & 1 & 1 & 1 \\ 0 & L & 0 & -L \\ -L & 0 & L & 0 \\ \frac{k_M}{k_F} & -\frac{k_M}{k_F} & \frac{k_M}{k_F} & -\frac{k_M}{k_F} \end{bmatrix} \begin{bmatrix} F_{i,1} \\ F_{i,2} \\ F_{i,3} \\ F_{i,4} \end{bmatrix}, \tag{2}$$

where L is the distance from the axis of rotation of the rotors to the center of the quadrotor. The total force and moments on the system from the quadrotors in the body frame coordinates, $\mathbf{B}$, are:

$$\begin{bmatrix} F_B \\ M_{xB} \\ M_{yB} \\ M_{zB} \end{bmatrix} = \sum_i \begin{bmatrix} 1 & 0 & 0 & 0 \\ y_i & cos\psi_i & -sin\psi_i & 0 \\ -x_i & sin\psi_i & cos\psi_i & 0 \\ 0 & 0 & 0 & 1 \end{bmatrix} \begin{bmatrix} F_{q,i} \\ M_{xq.i} \\ M_{yq.i} \\ M_{zq.i} \end{bmatrix}. \tag{3}$$

Note that z_i is not present in (3) so this formulation allows for quadrotors in different planes. If we let m be the mass of the entire system and ignore air drag, then the equations governing the acceleration of the center of mass are simply:

$$m\ddot{\mathbf{r}} = \begin{bmatrix} 0 \\ 0 \\ -mg \end{bmatrix} + {}^W R_B \begin{bmatrix} 0 \\ 0 \\ F_B \end{bmatrix}. \tag{4}$$

The moment of inertia matrix for the entire system referenced to the center of mass along the $x_B - y_B - z_B$ axes is denoted by I. We assume $x_B - y_B - z_B$ are chosen such that I is diagonal. The angular accelerations determined by the Euler equations are:

$$I \begin{bmatrix} \dot{p} \\ \dot{q} \\ \dot{r} \end{bmatrix} = \begin{bmatrix} M_{xB} \\ M_{yB} \\ M_{zB} \end{bmatrix} - \begin{bmatrix} p \\ q \\ r \end{bmatrix} \times I \begin{bmatrix} p \\ q \\ r \end{bmatrix}.$$

4 Control

4.1 Control Basis Vectors

The linear system in (3) defines four equations with $4n$ unknowns and can be rewritten as:

$$\left[F_B,\, M_{xB},\, M_{yB},\, M_{zB}\right]^{\mathrm{T}} = A\mathbf{u},$$

where $A \in \mathbb{R}^{4\times 4n}$ is fixed and determined by the relative positions and orientations of the n quadrotors. Here $\mathbf{u} \in \mathbb{R}^{4n}$ contains the four control inputs for each of the quadrotors:

$$\mathbf{u} = \left[F_{q,1}, M_{xq,1}, M_{yq,1}, M_{zq,1}, ..., F_{q,n}, M_{xq,n}, M_{yq,n}, M_{zq,n}\right]^T.$$

For a system with more than one quadrotor the linear system is underdetermined so we have a choice on how to achieve net forces and moments on the entire system. Here we choose an optimal control input $\mathbf{u}^*$ which achieves the desired net force and moments (F_B^{des}, M_{xB}^{des}, M_{yB}^{des}, and M_{zB}^{des}) while minimizing the cost function, J:

$$\mathbf{u}^* = \underset{\mathbf{u}}{\operatorname{argmin}}\{J | [F_B^{des}, M_{xB}^{des}, M_{yB}^{des}, M_{zB}^{des}]^{\mathrm{T}} = A\mathbf{u}\} \tag{5}$$

where

$$J = \sum_i w_{Fi}F_{q,i}^2 + w_{Mxi}M_{xq,i}^2 + w_{Myi}M_{yq,i}^2 + w_{Mzi}M_{zq.i}^2.$$

A natural way to treat the point-wise minimization of the function J is by choosing control inputs using the Moore-Penrose inverse. First we define $H \in \mathbb{R}^{4n\times 4n}$ so that $J = \|H\mathbf{u}\|_2^2$:

$$H = \operatorname{diag}\left(\sqrt{w_{F1}}, \sqrt{w_{Mx1}}, \sqrt{w_{My1}}, \sqrt{w_{Mz1}}, ..., \sqrt{w_{Fn}}, \sqrt{w_{Mxn}}, \sqrt{w_{Myn}}, \sqrt{w_{Mzn}}\right).$$

After algebraic manipulation we get:

$$\begin{aligned}\mathbf{u}^* &= H^{-1}(AH^{-1})^{+}[F_B^{des}, M_x^{des}, M_y^{des}, M_z^{des}]^{\mathrm{T}} \\ &= H^{-2}A^{\mathrm{T}}(AH^{-2}A^{\mathrm{T}})^{-1}[F_B^{des}, M_x^{des}, M_y^{des}, M_z^{des}]^{\mathrm{T}},\end{aligned} \tag{6}$$

where $^+$ denotes the Moore-Penrose inverse. It is instructive to the think of the columns of the matrix $H^{-1}(AH^{-1})^+$ as control basis vectors $\mathbf{u}_F$, $\mathbf{u}_{Mx}$, $\mathbf{u}_{My}$, and $\mathbf{u}_{Mz}$. Then the optimal control input can be written as:

$$\mathbf{u}^* = [\mathbf{u}_F, \mathbf{u}_{Mx}, \mathbf{u}_{My}, \mathbf{u}_{Mz}][F_B^{des}, M_x^{des}, M_y^{des}, M_z^{des}]^{\mathrm{T}}. \tag{7}$$

We now consider the special case in which all quadrotors are identical and axially symmetric meaning roll and pitch can be treated the same way. Indeed this is the case in our experimental testbed. In this case $w_{Fi} = w_F$, $w_{Mxi} = w_{Myi} = w_{Mxy}$, and $w_{Mzi} = w_{Mz}$. Consider the following term from (6) for this case:

$$AH^{-2}A^T = \begin{bmatrix} \frac{n}{w_F} & \frac{\sum y_i}{w_F} & -\frac{\sum x_i}{w_F} & 0 \\ \frac{\sum y_i}{w_F} & \frac{\sum y_i^2}{w_F} + \frac{n}{w_{Mxy}} & \frac{-\sum x_i y_i}{w_F} & 0 \\ -\frac{\sum x_i}{w_F} & \frac{-\sum x_i y_i}{w_F} & \frac{\sum x_i^2}{w_F} + \frac{n}{w_{Mxy}} & 0 \\ 0 & 0 & 0 & \frac{n}{w_{Mz}} \end{bmatrix}. \tag{8}$$

Here we can assume that the positions of the quadrotors dominate the mass properties of the entire structure since the quadrotors are heavier than what they can carry. The x and y

locations of the center of mass of the payload and quadrotors together are close to that of just the quadrotors so $\sum x_i = \sum y_i = 0$. Additionally, $\sum x_i y_i = 0$, as the principle axes of the quadrotors are aligned with the principal axes of the structure. Therefore, all quadrotors contribute an equal force and yaw moment to produce a net body force or yaw moment:

$$\mathbf{u}_F = \frac{1}{n}\left[1, 0, 0, 0, ..., 1, 0, 0, 0\right]^{\mathrm{T}}$$
$$\mathbf{u}_{Mz} = \frac{1}{n}\left[0, 0, 0, 1, ..., 0, 0, 0, 1\right]^{\mathrm{T}}.$$

The control basis vectors for moments in pitch and roll reflect the tradeoff between the weighting factors:

$$\mathbf{u}_{Mx} = \frac{1}{\frac{w_{Mxy}}{w_F}\sum y_i^2 + n}\left[\frac{w_{Mxy}}{w_F}y_1, c\psi_1, s\psi_1, 0, ..., \frac{w_{Mxy}}{w_F}y_n, c\psi_n, s\psi_n, 0\right]^{\mathrm{T}}$$
$$\mathbf{u}_{My} = \frac{1}{\frac{w_{Mxy}}{w_F}\sum x_i^2 + n}\left[-\frac{w_{Mxy}}{w_F}x_1, -s\psi_1, c\psi_1, 0, ..., -\frac{w_{Mxy}}{w_F}x_n, -s\psi_n, c\psi_n, 0\right]^{\mathrm{T}}.$$

Here, an increase in the cost of individual quadrotor moments relative to the forces, w_{Mxy}/w_F, causes the individual body forces used to create a net body moment to increase and the individual body moments from each quadrotor to decrease. This ratio allows a user to tradeoff between the individual quadrotor force and moments used to create body moments in pitch and roll.

4.2 Attitude Control

To control the attitude of the body we use proportional derivative control laws that take the form:

$$\begin{aligned} M_{xB}^{\text{des}} &= k_{p,\phi}(\phi^{\text{des}} - \phi) + k_{d,\phi}(p^{\text{des}} - p) \\ M_{yB}^{\text{des}} &= k_{p,\theta}(\theta^{\text{des}} - \theta) + k_{d,\theta}(q^{\text{des}} - q) \\ M_{zB}^{\text{des}} &= k_{p,\psi}(\psi^{\text{des}} - \psi) + k_{d,\psi}(r^{\text{des}} - r). \end{aligned} \tag{9}$$

4.3 Hover Controller

Here we use pitch and roll angle to control position in the x_W and y_W plane, M_{zB}^{des} to control yaw angle, and F_B^{des} to control position along z_W. This approach is similar to that used for individual quadrotors in [10–12]. We let $\mathbf{r}_T(t)$ and $\psi_T(t)$ be the trajectory and yaw angle we are trying to track. Note that $\psi_T(t) = \psi_0$ for the hover controller. The command accelerations, $\ddot{\mathbf{r}}^{\text{des}}$, are calculated from PID feedback of the position error, $\mathbf{e} = (\mathbf{r}_T - \mathbf{r})$, as:

$$(\ddot{\mathbf{r}}_T - \ddot{\mathbf{r}}^{\text{des}}) + K_d(\dot{\mathbf{r}}_T - \dot{\mathbf{r}}) + K_p(\mathbf{r}_T - \mathbf{r}) + K_i\int(\mathbf{r}_T - \mathbf{r}) = \mathbf{0},$$

where $\dot{\mathbf{r}}_T = \ddot{\mathbf{r}}_T = \mathbf{0}$ for hover. We linearize (4) to get the relationship between the desired accelerations and roll and pitch angles:

$$\begin{aligned} \ddot{r}_1^{\text{des}} &= g(\theta^{\text{des}}\cos\psi_T + \phi^{\text{des}}\sin\psi_T) \\ \ddot{r}_2^{\text{des}} &= g(\theta^{\text{des}}\sin\psi_T - \phi^{\text{des}}\cos\psi_T) \\ \ddot{r}_3^{\text{des}} &= \frac{1}{m}F_B^{\text{des}} - g. \end{aligned}$$

These relationships are inverted to compute the desired roll and pitch angles for the attitude controller, from the desired accelerations, as well as F_B^{des}:

$$\begin{aligned}\phi^{\text{des}} &= \frac{1}{g}(\ddot{r}_1^{\text{des}} \sin\psi_T - \ddot{r}_2^{\text{des}} \cos\psi_T) \\ \theta^{\text{des}} &= \frac{1}{g}(\ddot{r}_1^{\text{des}} \cos\psi_T + \ddot{r}_2^{\text{des}} \sin\psi_T) \\ F_B^{\text{des}} &= m(\ddot{r}_3^{\text{des}} + g).\end{aligned}$$

We substitute these into (9) to yield the desired net body force and moments. From these quantities the control inputs for individual quadrotors are computed using the control basis vectors developed in Sec. 4.1:

$$\mathbf{u} = F_B^{\text{des}}\mathbf{u}_F + M_{xB}^{\text{des}}\mathbf{u}_{Mx} + M_{yB}^{\text{des}}\mathbf{u}_{My} + M_{zB}^{\text{des}}\mathbf{u}_{Mz}.$$

We then calculate the desired angular velocities for each of the $4n$ rotors from a linearization of (1,2) about the nominal hovering operating point.

4.4 3D Trajectory Control

The trajectory controller is used to follow 3D trajectories with modest accelerations so the near-hover assumptions hold. We use an approach similar to those described in [12, 13]. We have a method for calculating the closest point on the trajectory, $\mathbf{r}_T$, to the the current position, $\mathbf{r}$. Let the unit tangent vector of the trajectory associated with that point be $\hat{\mathbf{t}}$ and the desired velocity vector be $\dot{\mathbf{r}}_T$. We define the position and velocity errors as:

$$\mathbf{e}_p = ((\mathbf{r}_T - \mathbf{r}) \cdot \hat{\mathbf{n}})\hat{\mathbf{n}} + ((\mathbf{r}_T - \mathbf{r}) \cdot \hat{\mathbf{b}})\hat{\mathbf{b}}$$

and

$$\mathbf{e}_v = \dot{\mathbf{r}}_T - \dot{\mathbf{r}}.$$

Note that here we ignore position error in the tangent direction by only considering position error in the normal, $\hat{\mathbf{n}}$, and binormal, $\hat{\mathbf{b}}$, directions. This is done because we are more concerned about reducing the cross-track error rather than error in the tangent direction of the trajectory.

We calculate the commanded acceleration, $\ddot{\mathbf{r}}^{\text{des}}$, from PD feedback of the position and velocity errors:

$$\ddot{\mathbf{r}}^{\text{des}} = K_p\mathbf{e}_p + K_d\mathbf{e}_v + \ddot{\mathbf{r}}_T.$$

Note that $\ddot{\mathbf{r}}_T$ represents feedforward terms on the desired accelerations. At low accelerations these terms can be ignored but at larger accelerations they can significantly improve controller performance. Finally, we use the process described in Sec. 4.3 to compute the desired angular velocities for each rotor.

4.5 Decentralized Control Law

We assume the quadrotors are attached rigidly to the body. As long as each quadrotor knows its fixed relative position and orientation with respect to the body and the goal of the body controller (hover location or desired trajectory) then this controller can be decentralized. If each quadrotor senses its own orientation and angular velocity then the orientation and angular velocity of the body are calculated as follows:

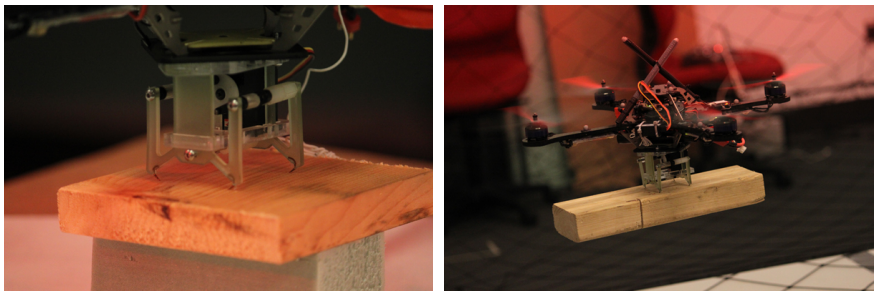

(a) (b)

Fig. 2. Gripping mechanism engaged in wood. The assembly consists of a compliant polymer with embedded opposed microspines, linkages, and a servo mechanism for engaging and releasing (Fig. 2(a)). The gripping mechanism is attached to each quadrotor (Fig. 2(b)).

$$ {}^{W}R_{B} = {}^{W}R_{Q_i}\,{}^{Q_i}R_{B} \quad \text{and} \quad [p,q,r]^{\mathrm{T}} = {}^{B}R_{Q_i}[p_i,q_i,r_i]^{\mathrm{T}}. $$

From the position and velocity of the i^{th} quadrotor, the position and velocity of the center of mass of the body are calculated as:

$$ \begin{aligned} \mathbf{r} &= \mathbf{r}_i - {}^{W}R_{B}[x_i,y_i,z_i]^{\mathrm{T}} \\ \dot{\mathbf{r}} &= \dot{\mathbf{r}}_i - \omega_{\mathbf{B}} \times \left({}^{W}R_{B}[x_i,y_i,z_i]^{T}\right). \end{aligned} $$

Each quadrotor then runs a local hover or velocity controller along with the attitude controller (9).

For completely centralized control, the state estimates of the n quadrotors are combined to create a single estimate of the state of the entire body from which the control inputs are computed. This averaging reduces the noise on the state estimate of the entire body and thus results in a cleaner control signal.

For the results presented in this work, we use a combination of the decentralized and centralized formulations. The position, velocity, and orientation estimates all come from a single source so the terms in the control input that depend on these values are calculated in a centralized fashion. The angular velocity is measured directly onboard each quadrotor so the terms in the control law that depend on the angular velocity are calculated using the decentralized method.

5 Gripping Mechanism

The gripping mechanism shown in Fig. 2 enables the quadrotors to attach to and release from the payload. The design is specialized to allow gripping of horizontal planar surfaces. This design choice is motivated by the problem definition, as all quadrotors are expected to attach to parallel horizontal planes with respect to the payload. It is also desirable for the gripper to be able to engage at any point on suitable materials. This gripper is designed to penetrate surfaces via opposed microspines actuated by a servo motor. Opposed spines allow large shear forces, which in turn allow a large normal force.

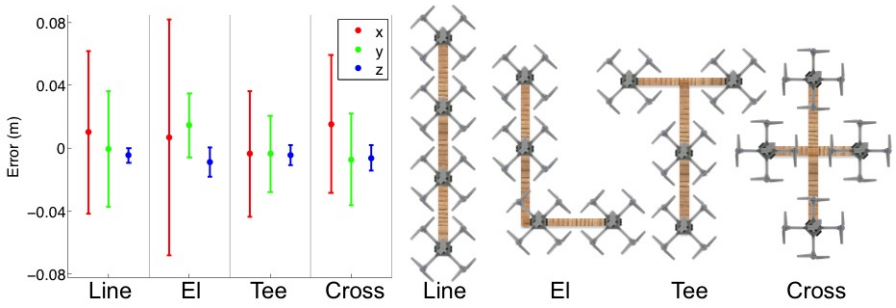

Fig. 3. Hover performance data for 40 seconds for four configurations. The center dot represents the mean error and the error bars represent one standard deviation. Graphical depictions of the four configurations.

The gripper penetrates the surface of an object by driving four hooks into the plane with a servo motor. The hooks are standard fishing hooks which are accessible, cheap, sharp, and sufficiently strong for use in this application. Locating the hooks precisely with respect to the quadrotor is important as the the top face of the object must remain parallel to the quadrotor. To this end, we employ shape deposition manufacturing (SDM) to manufacture the full spine. The resulting compliant polymer spine introduces assistive compliance into the gripper. When the servo opens the gripper, the polymer acts as a spring that when released, aids the servo in penetrating the surface. After some penetration is achieved, the piece passes through its natural state and is stretched in the opposite direction. The piece responds with a restoring force that assists the servo on releasing the surface. We tested the gripping mechanism with a number of materials and found it to be effective in grasping soft to medium hardness woods, cardboard, high density foam, and carpet.

6 Results

In this section we describe results from two experimental trials designed to evaluate the performance of the controllers described in Sect. 4.3 and demonstrate cooperative grasping, manipulation, and transportation of payloads in 3D.

The hardware, software, and implementation details of the experiments follows. The position and orientation of the quadrotor is observed using a VICON motion capture system operating at 100 Hz [14]. The position is numerically differentiated to compute the linear velocity of the robot while the angular velocity is sensed onboard the quadrotor with a 3-axis rate gyro. The position, linear velocity, and orientation are available to MATLAB via ROS [15] and a ROS-MATLAB bridge [16]. All commands are computed in MATLAB using the latest state estimate at the rate of the VICON. The commands in MATLAB are bridged to ROS and the most recent command is sent to the robot via ZIGBEE at a fixed rate of 100 Hz. This fixed rate is due to the limited bandwidth of ZIGBEE (57.6 kbps). Commands sent to the robot consist of the gains, desired attitude, and thrust values described in Sect. 4.

The first experimental trial consists of a team of four quadrotors rigidly attached to different payload configurations (see Figures 3 and 5). For this test, we wish to focus on co-

Configuration	I_{xx} (kg m^2)	I_{yy} (kg m^2)	m (kg)
Line	0.0095	0.73	3.33
El	0.079	0.50	3.33
Tee	0.082	0.43	3.33
Cross	0.11	0.19	3.23

Table 1. Mass and Inertia Properties.

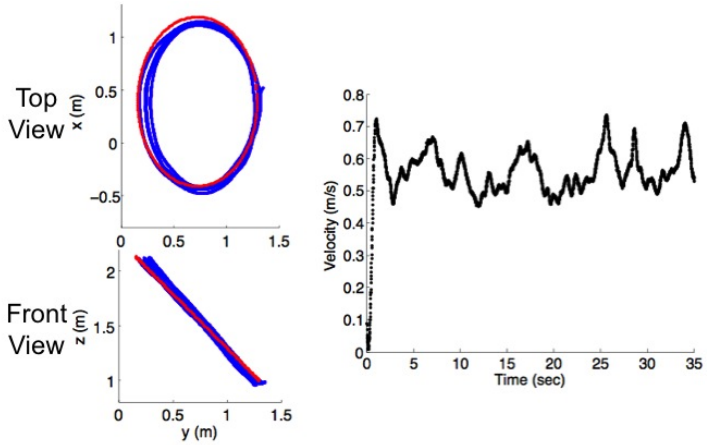

Fig. 4. Trajectory tracking data for the *Cross* configuration along a $0.8,$ m radius circle tilted at 45° from horizontal at 0.6 m/s.

operative manipulation and transportation and as such use a payload structure built of wood with quadrotors attachments made via Velcro for easy rearranging. The total mass and x and y principal moments of inertia for each configuration (payload and quadrotors) are shown in Table 1. Note that the mass of a single quadrotor with a battery is about 500 g, so in each of these configurations the total payload is greater than 1.2 kg.

For each configuration, the control basis vectors are computed as described in Sect. 4.1 with $w_{Mxy}/w_F = 2$. We chose this ratio as our connection to the payload is stronger in resisting a force pulling it away from a surface than a moment in pitch or roll. Data for each configuration is shown in Fig. 3. Note that for each configuration, control along the x axis is intentionally performed with the body angle corresponding to the larger principal moment of inertia, I_{yy}. The performance along the x axis is worse than the y axis as expected. A large moment of inertia limits the bandwidth of the control on that angle. This decrease in attitude control performance leads to decreased position control performance along that axis. Here we note that position control for a single quadrotor is much better than for any of the multi-robot structures because their moments of inertia are much larger.

The trajectory tracking controller in Sect. 4.4 is implemented on the *Cross* configuration for which data is shown in Fig. 4. We see that the system performs well and controls to the desired trajectory in three-dimensions.

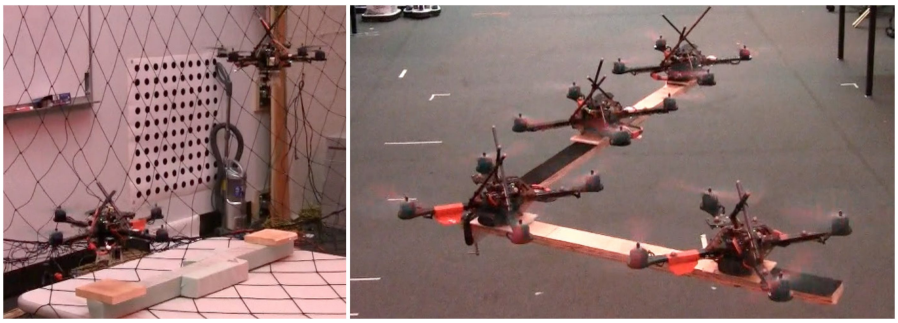

Fig. 5. Left: Image from an experiment with the gripping mechanism enabling cooperative grasping, manipulation, and transportation. Right: Four quadrotors carrying a payload in the *El* configuration. Videos of the experiments are available at http://tinyurl.com/penndars.

The gripping mechanism described in Sect. 5 is used on two quadrotors to pick up and transport an $0.8\,\mathrm{m}$, $320\,\mathrm{g}$ structure as shown in Fig. 5. The quadrotors first descend to the structure and engage the gripping mechanism. The quadrotors ascend with the structure and fly twice along the same circular trajectory as in Fig. 4 at $0.5\,\mathrm{m/s}$. Finally, the quadrotors descend to structures initial location, disengage the gripping mechanism, and depart.

7 Conclusions and Future Work

We addressed the problem of controlling multiple quadrotor robots that cooperatively grasp, manipulate, and transport a payload in three dimensions. We approach the problem by first developing a model for a single quadrotor and a team of quadrotors rigidly attached to a payload. We propose individual robot control laws defined with respect to the payload that stabilize the payload along three-dimensional trajectories. We detail the design of a gripping mechanism attached to each quadrotor that permits autonomous grasping of the payload. We conclude with an experimental study with teams of quadrotors cooperatively grasping, stabilizing, and transporting payloads of different configurations to desired positions and along three-dimensional trajectories.

We are currently working on autonomous system identification methods for multiple quadrotors picking up payloads with unknown masses and moments of inertia. We also plan to modify the gripping mechanism design to enable passive engagement so that a quadrotor can simply land on a surface to attach to it.

8 Acknowledgements

We would like to acknowledge Mark Cutkosky, Alexis Desbiens, Alan Asbeck, and Ben Kallman for their input in the choice of gripping strategies.

References

1. N. Michael, J. Fink, and V. Kumar, "Cooperative manipulation and transportation with aerial robots," in *Proc. of Robotics: Science and Systems*, Seattle, WA, June 2009.
2. J. Fink, N. Michael, S. Kim, and V. Kumar, "Planning and control for cooperative manipulation and transportation with aerial robots," in *Proc. of the Int. Symposium of Robotics Research*, Luzern, Switzerland, Aug. 2009.
3. K. Salisbury and B. Roth, "Kinematics and force analysis of articulated mechanical hands," *J. Mechanisms, Transmissions, and Automation in Design*, vol. 105, pp. 35–41, Dec. 1983.
4. A. Bicchi and V. Kumar, "Robotic grasping and contact," in *Proc. of the IEEE Int. Conf. on Robotics and Automation*, San Francisco, CA, Apr. 2000, pp. 348–353.
5. V. Kumar and K. J. Waldron, "Analysis of omnidirectional gaits for walking machines for operation on uneven terrain," in *Proc. of Sym. on Theory and Practice of Robots and Manipulators*, Udine, Italy, Sept. 1988, pp. 37–62.
6. R. Oung, F. Bourgault, M. Donovan, and R. D'Andrea, "The distributed flight array," in *Proc. of the IEEE Int. Conf. on Robotics and Automation*, Anchorage, AK, May 2010, pp. 601–607.
7. "Ascending Technologies, GmbH," http://www.asctec.de.
8. A. T. Asbeck, S. Kim, and M. R. Cutkosky, "Scaling hard vertical surfaces with compliant microspine arrays," in *Proc. of Robotics: Science and Systems*, Cambridge, MA, June 2005.
9. A. L. Desbiens and M. R. Cutkosky, "Landing and perching on vertical surfaces with microspines for small unmanned air vehicles," *J. Intell. Robotic Syst.*, vol. 57, pp. 313–327, Jan. 2010.
10. S. Bouabdallah, "Design and control of quadrotors with applications to autonomous flying," Ph.D. dissertation, Ecole Polytechnique Federale de Lausanne, Lausanne, Switzerland, Feb. 2007.
11. D. Gurdan, J. Stumpf, M. Achtelik, K. Doth, G. Hirzinger, and D. Rus, "Energy-efficient autonomous four-rotor flying robot controlled at 1 khz," in *Proc. of the IEEE Int. Conf. on Robotics and Automation*, Roma, Italy, Apr. 2007.
12. N. Michael, D. Mellinger, Q. Lindsey, and V. Kumar, "The GRASP multiple micro UAV testbed," *IEEE Robotics and Automation Magazine*, Sept. 2010.
13. G. Hoffmann, S. Waslander, and C. Tomlin, "Quadrotor helicopter trajectory tracking control," in *AIAA Guidance, Navigation and Control Conference and Exhibit*, Honolulu, Hawaii, Apr. 2008.
14. "Vicon Motion Systems, Inc." http://www.vicon.com.
15. "Robot Operating System (ROS)," http://www.ros.org.
16. "ROS-Matlab Bridge," http://github.com/nmichael/ipc-bridge.